GEOPHYSICAL RESEARCH LETTERS, VOL. 19, NO. 3, PAGES 301-304, FEBRUARY 7, 1992

TSUNAMI FROM THE MARIANA EARTHQUAKE OF APRIL 5, 1990: ITS ABNORMAL PROPAGATION AND IMPLICATIONS FOR TSUNAMI POTENTIAL FROM OUTER-RISE EARTHQUAKES

Kenji Satake
Department of Geological Sciences, University of Michigan

Yasuhiro Yoshida and Katsuyuki Abe
Earthquake Research Institute, University of Tokyo

Abstract. The tsunami generated by the Mariana earthquake of April 5, 1990 was observed on the Japanese and Pacific islands as far as Hawaii. The observed tsunami amplitudes are not a simple function of distance from the source but vary with large-scale bathymetry. Numerical computations of tsunami propagation are made for actual bathymetry and the computed amplitudes are compared with the observations. From the comparisons, the seismic moment is estimated to be 1.4×10^{20} Nm, very similar to that from seismic waves, and indicates that the seismic waves and tsunami are equally excited. The numerical computations also show that the tsunami propagated toward the Japanese coast through two different paths: one is through the trench system with high velocity and small amplitude, the other along the ridge system with low velocity but large amplitude. The two kinds of tsunami are identified on recently-installed ocean bottom pressure gauges. Since the Mariana earthquake was an outer-rise earthquake in a weakly coupled subduction zone, where the size of outer-rise event is larger than underthrusting events, it is possible that even larger earthquakes occur in this region. The tsunami potential from such events must be considered, including the unusual tsunami propagation.

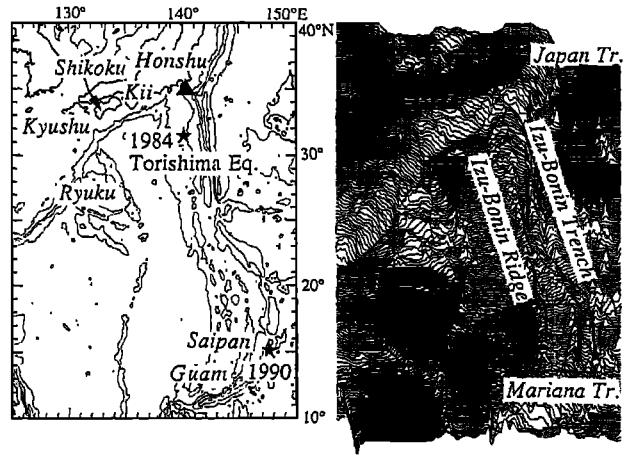

Fig. 1. Topography around the Izu-Bonin-Mariana trench system. The computation of tsunami is made in this area with a grid size of 1 min. The star symbols show the sources of the 1984 Torishima and 1990 Mariana tsunamis. The solid triangle shows approximate location of ocean bottom tsunami gauges and tide gauge (Mera) that record trench and ridge waves. The contour interval for bathymetry is 2000 m.

Introduction

A moderate-size tsunami was caused by an earthquake that occurred in the Mariana region on April 5, 1990. Although the size of the tsunami was not large enough to cause damage, it was clearly recorded on tide gauges on the Japanese coast and in the Pacific islands as far as Hawaii. The amplitude of the tsunami shows abnormal geographical distribution.

The earthquake occurred at the deep Mariana trench (Figure 1) where the oldest part of the Pacific plate is subducting beneath the Philippine Sea plate. A series of trenches (Mariana and Izu-Bonin trenches) extends from the source area to the north up the Japanese coast. A ridge (Izu-Bonin ridge) system runs parallel to the west. These topographic features might have affected the tsunami propagation.

An unusual tsunami was also observed from the 1984 Torishima earthquake which occurred on the Izu-Bonin ridge. Satake and Kanamori [1991] found that the abnormally large tsunami from the Torishima event was due to both the abnormal propagation along the ridge system and an unusual source process with a non-fault origin, most likely an injection of material into a shallow sediment layer.

The source process of the Mariana earthquake was investigated in detail by Yoshida et al.[1992]. They found that the earthquake was caused by a normal fault motion within the subducting Pacific plate. The seismic moment was 1.4 x 10^{20} Nm or M_W=7.3. This earthquake is an example of an outer-rise event in a subduction zone where the seismic coupling between subducting and overlying plates is weak.

In this paper, we make numerical computations of the tsunami on actual bathymetry. The tsunami source model can be estimated from the comparison between the computed and observed tsunami amplitudes. The numerical computations also show the bathymetric effect on the tsunami propagation. We further discuss future tsunami potential from an earthquake in this region.

Observed Tsunami

The tsunami from the Mariana earthquake was recorded on many tide gauges in Japan as well as in Truk (the maximum peak-to-peak amplitude was 3 cm), Wake Island (4 cm), Midway (6 cm) and Kailua-Kona on the Island of Hawaii (24 cm). Figure 2 shows the maximum amplitudes of tsunami observed on tide gauges in Japan. The figure also shows the tsunami heights computed by a method we will discuss later. The tsunami amplitude is large on the islands along the Izu-Bonin ridge system, ranging from 18 cm at Izu-Oshima to 42 cm at Kozu-jima. On the southern coast of Japan, the

Paper number 91GL02493
0094-8534/92/91GL-02493$03.00

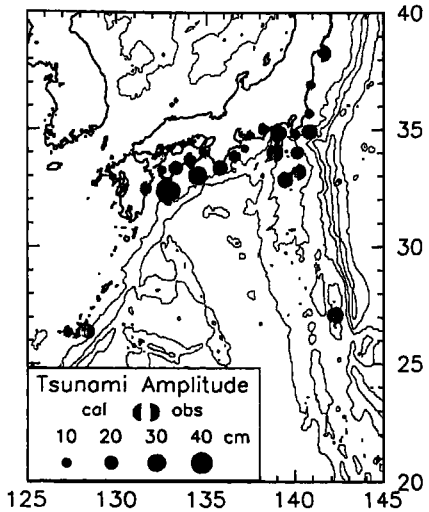

Fig. 2. The maximum amplitudes of observed and computed tsunamis. The source of the Mariana earthquake is far south of this map.

amplitude is as large as 30 to 50 cm on the southern tip of Kii peninsula and the southeastern and southwestern tips of Shikoku. On the other parts of the Japanese coast, the amplitude is smaller than 20 cm. Part of the variation in tsunami amplitude may be due to local (scale length of less than a few km) topography. Figure 2 indicates, however, that larger-scale topography determines the general pattern of tsunami amplitudes.

Computation of Tsunami

From the analysis of seismic surface and body waves, and aftershock distribution, the fault parameters of this earthquake are estimated as follows [Yoshida et al., 1992]. The strike is 198°, the dip angle is 48° (dipping to the west), the slip angle is -90° (pure normal faulting). The aftershock area extends as long as 70 km along the strike and as deep as 36 km. On the other hand, the detailed analysis of body waves shows that the rupture area may be much smaller. The short duration, about 10 sec, of the source process inferred from body waves suggests that the rupture length may be as short as 40 km.

Based on the above results of seismic analysis, we assume two different fault models. The longer fault model is 70 km × 40 km while the shorter model is 40 km × 25 km. The former includes the whole aftershock area while the latter covers the area between the two aftershock clusters where the aftershocks are relatively sparse [Yoshida et al., 1992]. The top edge of the fault is assumed to be 10 km beneath the ocean bottom. The deformation on the ocean bottom is computed for a unit amount of slip and is used for an initial condition of tsunami propagation. The average slip on the fault will be estimated by matching the observed and computed tsunami amplitudes.

We compute the tsunami propagation numerically on actual bathymetry. The equation of motion of linear long-wave and the equation of continuity are solved by a finite-difference method in a spherical coordinate system [Hwang et al., 1972; Kowalik and Murty, 1984]. The computational area is the same as shown in Figure 1 with the grid size of 1 min of arc, or about 2 km, small enough to incorporate the fine bathymetry including the trench and ridge systems. The total number of grid points is 1500 × 1800. The computations were made for 10 hours after the origin time with a time step of 4 seconds.

The tsunami waveforms are calculated at the grid points corresponding to tide gauge stations. The computed maximum amplitudes are compared with the observed ones. The geometric average K of the amplitude ratio O_i/C_i, where O_i and C_i are the observed and computed amplitudes at the i-th station, is calculated and used to estimate the average slip on the fault. The average slip on the fault can be estimated so that the average K becomes unity. An index of scattering κ, as defined by Aida [1978] as

$$\log \kappa = \left[\frac{1}{n} \sum_i (\log \frac{O_i}{C_i})^2 - (\log K)^2 \right]^{1/2}$$

is also calculated to judge the fit of model to data. If the amplitude ratio is the same at all the stations, κ becomes unity. The larger κ means the larger scatter.

Tsunami Source Model

For the fault model with a size of 70 km × 40 km, the slip is estimated as 1.5 m. The scatter, κ, is 2.08. For the fault model with 40 km × 25 km, the slip is estimated as 3.4 m. The value of κ is 1.96, slightly smaller than that of the larger fault. From the tsunami amplitude comparisons, the smaller fault is preferable to the larger fault, although the difference does not seem to be significant. The average slip of 3.4 m on 40 km × 25 km corresponds to the seismic moment of 1.4 × 10^{27} dyne-cm (10^{20} Nm) assuming that the rigidity is 4 × 10^{11} dyne/cm^2. This value is the same as that from seismic wave analysis [Yoshida et al., 1992], indicating that the fault model provides a consistent explanation for both seismic and tsunami waves. This is in contrast to the 1984 Torishima earthquake for which tsunami excitation was much larger than expected from the seismic wave analysis [Satake and Kanamori, 1991].

Figure 2 shows the computed amplitudes compared to the observed ones. The geographical distribution of amplitudes, including the large tsunamis on the ridge system and at the tips of peninsulas, is well reproduced. This indicates that the tsunami amplitudes are determined by bathymetry with a scale length of 1 min (about 2 km) or larger.

Tsunami Propagation

Figure 3 shows the water height distributions near the source area at 10, 20 and 30 minutes after the origin time. The initial water surface disturbance is predominantly a depression in an area of about 50 km × 25 km with a maximum amplitude of 120 cm. The tsunami source area is elliptically shaped with the major axis in the north-south direction because the fault extends along the trench axis. At 10 minutes after the origin time, the disturbance area is still elliptically shaped, extending north-south along the trench. As the tsunami travels fast north- and southward, the water surface disturbance is elongated in the north-south direction. The tsunami travels slower in the direction perpendicular to the trench, because of shallower depth, and the amplitude becomes larger. This feature can be seen at 20 and 30 minutes. At 30 minutes, the tsunami traveling to the west arrived at the ridge, where the velocity is less than half that

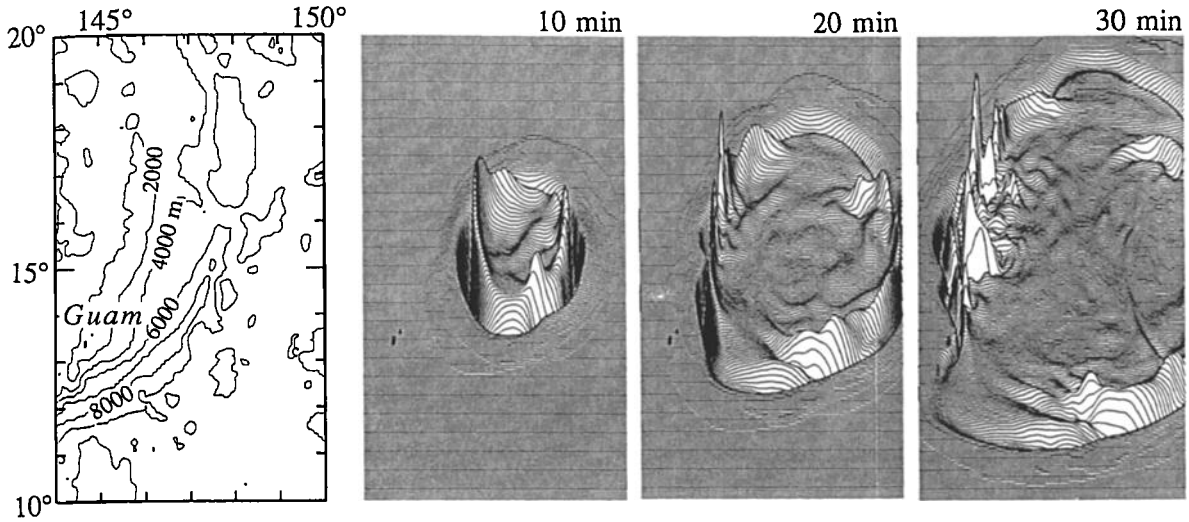

Fig.3. The bathymetry and snapshots of computed tsunami heights near the source. The vertical scale is exaggerated by 10^5, or the maximum amplitude at 30 min is about 250 cm.

along the trench, and the amplitude becomes much larger. The large amplitude tsunami on the ridge forms a kind of secondary source, then starts traveling along the ridge system. We also computed the tsunami propagation from a source with circular shape. The tsunami propagation and the amplitude distributions are very similar to that from the fault model, indicating that the directivity is due to bathymetric effect, not due to the shape of the source area. The source area of this event may be too small to produce directivity due to the shape of the source area.

Figure 4 shows the tsunami heights at 1, 2, 3 and 4 hours after the origin time in the whole computational area. The tsunami travels faster along the trench system with small amplitude. We will call this a trench wave. From the secondary source on the ridge, the tsunami travels towards northwest with large amplitude. At 2 hours, two peaks can be seen: one is heading towards Kyushu and Shikoku, the other is still traveling along the ridge system. The tsunami energy is trapped by the ridge system. This is a kind of edge wave and has been proposed theoretically but does not seem to have been observed before [LeBlond and Mysak, 1978]. We will call this a ridge wave. At 3 hours, the largest amplitude tsunami is approaching Shikoku. At 4 hours, the ridge wave is still traveling northward along the ridge system.

Recently several ocean bottom pressure gauges have been installed on the deep ocean bottom off the Japanese coast and the data are telemetered by cable [Okada, 1991]. Both the trench and ridge waves were observed on one of the ocean bottom pressure gauges and a few tide gauge stations along the ridge system. Figure 5 shows the observed and computed tsunami waveforms on the two ocean bottom pressure gauges (Boso-1 and Boso-3) and the tide gauge at Mera. The location of these gauges is shown by a solid triangle in Figure 1. All the records are high-pass filtered with a cutoff period of 20 minutes. The ocean depth at the pressure gauge Boso-1 is 4011 m and 1912 m at Boso-3 [Okada, 1991], so the tsunami amplitudes are much smaller than those seen on standard tide gauges in the coastal region. The computed waveforms clearly show the first arrival around 3 hours with small amplitude and a large amplitude later phase at about 4.5 hours. Referring to Figure 4, these are identified as the trench wave and ridge wave, respectively. The observed waveforms

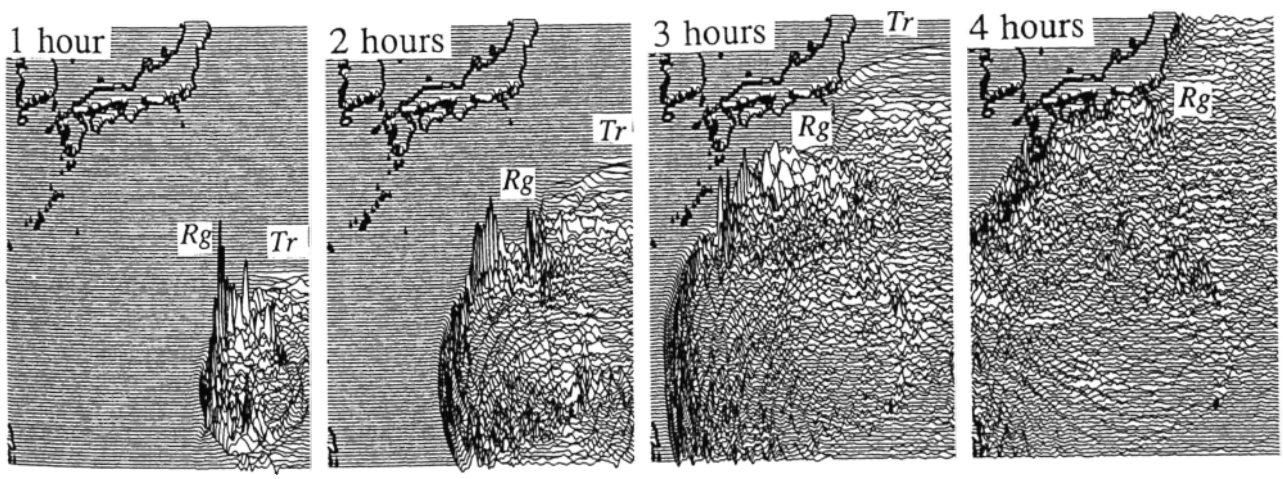

Fig. 4. The snapshots of tsunami propagation at 1, 2, 3 and 4 hours after the origin time. The vertical scale is exaggerated by 10^5, or the land height corresponds to 10 cm of tsunami amplitude. The trench (*Tr*) and ridge (*Rg*) waves are clearly seen.

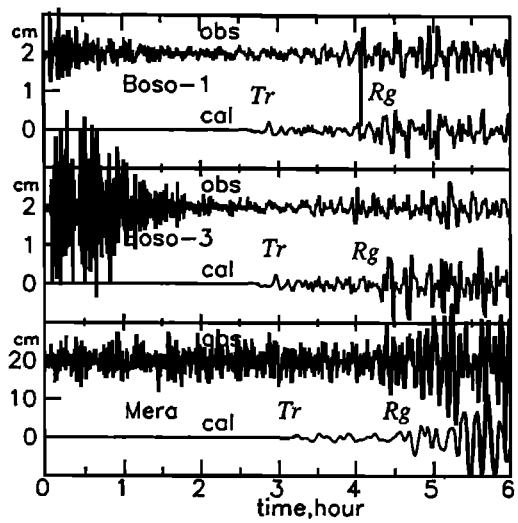

Fig. 5. Comparison of the observed and computed tsunami waveforms on two ocean bottom tsunami gauges (Boso-1 and 3) and tide gauge at Mera (see Fig.1 for location). Two kinds of waves, trench (*Tr*) and ridge (*Rg*) waves, are seen.

are very noisy, but the ridge waves are apparent in all the records. On Boso-3, the arrival of the trench wave can be seen just before the time mark of 3 hours. At the other two stations, the arrival of trench waves may be buried in the noise.

Implication for Future Tsunami Potential

The Mariana earthquake is an outer-rise event which is defined as an earthquake occurring within the oceanic plate in the vicinity of the trench axis. Christensen and Ruff [1988] proposed a model in which the stress regime in the outer rise varies both temporally and spatially due to cyclic influences of large underthrusting earthquakes on the regional stress. In their model, the outer rise stress field in a coupled zone is compressional before large underthrusting earthquakes but becomes tensional after the large underthrusting events. In an uncoupled zone, on the other hand, the outer rise earthquakes are always normal faulting events, indicating a tensional stress field, without any correlation to subduction zone seismicity. The 1990 event was the largest earthquake since 1902 in the Marianas [Yoshida et al., 1992]. Considering the short period of seismological observation compared to geologic time scale, there is no reason to believe that the 1990 earthquake was the largest possible size. In the Sunda arc, another subduction zone where the coupling is also weak, a much larger earthquake (M_w 8.2-8.3) occurred in 1977. This event, the Sumbawa earthquake, is another example of an outer-rise event [Christensen and Ruff, 1988] and the largest earthquake in the region ever recorded. These indicate that the largest earthquake in an uncoupled subduction zone is an outer rise earthquake rather than an underthrusting event.

This has important implications to future hazard assessment, particularly from tsunamis, since most hypothetical tsunamis have been assumed to be generated from underthrusting events associated with subduction. A hypothetical tsunami from an earthquake with a seismic moment five times larger than the 1990 event (M_w=7.9) can be modeled by making the average slip 7.5 m in a fault area of 70 km × 40 km. Since both the ocean bottom deformation and the tsunami propagation are linear processes, when the slip on the fault is five time times larger, the tsunami amplitudes on Japanese and Pacific Islands also becomes five times larger. This means that tsunami amplitudes on Shikoku, Izu Islands and Hawaii would exceed 2 m, which could cause moderate damage to coastal areas.

The lack of large underthrusting earthquakes in weakly coupled subduction zones like the Marianas does not mean that earthquake and tsunami potentials are low. For tsunami potential, the unusual propagation must also be accounted for in hazard assessments.

Acknowledgments. We thank Masami Okada at Meteorological Research Institute for providing us the tide gauge and ocean bottom pressure gauge records. Toshiyuki Hibiya, Larry Ruff, Roland LaForge and Jean Johnson kindly reviewed the manuscript and provided valuable comments.

References

Aida, I., Reliability of a tsunami source model derived from fault parameters, *J. Phys. Earth*, 26, 57-73, 1978.

Christensen, D.H. and L. Ruff, Seismic coupling and outer rise earthquakes, *J. Geophys. Res.*, 13, 13421-13444, 1988.

Hwang, L-S. and D. Divoky, Tsunami generation, *J. Geophys. Res.*, 75, 6802-6817, 1970.

Kowalik, Z. and T. Murty, Computation of tsunami amplitudes resulting from a predicted major earthquake in the Shumagin seismic gap, *Geophys. Res. Lett.*, 11, 1243-1246, 1984.

LeBlond, P.H. and L.A. Mysak, *Wave in the Ocean*, Elsevier Scientific Publishing Company, 1978.

Okada,. M., Ocean bottom pressure gauge for tsunami warning system in Japan, *Proc. 2nd UJNR Tsunami Workshop*, 219-227, National Geophysical Data Center, NOAA, Boulder, CO, 1991.

Satake, K. and H. Kanamori, Abnormal tsunamis caused by June 13, 1984 Torishima, Japan, earthquake, *J. Geophys. Res.*, 96, 19933-19939, 1991.

Yoshida, Y., K. Satake, and K. Abe, The large normal-faulting Mariana earthquake of April 5, 1990 in uncoupled subduction zone, *Geophys. Res. Lett., this issue*, 1992.

K. Abe and Y. Yoshida, Earthquake Research Institute, University of Tokyo, Yayoi, Bunkyo-ku, Tokyo, 113 Japan.

K. Satake, Department of Geological Sciences, University of Michigan, 1006 C. C. Little Building, Ann Arbor, MI 48109.

(Received August 27, 1991;
accepted September 17, 1991.)